Biosensors and Bioelectronics 132 (2019) 97–104

Contents lists available at ScienceDirect

Biosensors and Bioelectronics

journal homepage: www.elsevier.com/locate/bios

A prostate-specific antigen electrochemical immunosensor based on Pd NPs functionalized electroactive Co-MOF signal amplification strategy

Li Dai[a], Yueyuan Li[a], Yaoguang Wang[a], Xiliang Luo[b], Dong Wei[c], Rui Feng[c], Tao Yan[c], Xiang Ren[a], Bin Du[c], Qin Wei[a,*]

[a] Key Laboratory of Interfacial Reaction & Sensing Analysis in Universities of Shandong, School of Chemistry and Chemical Engineering, University of Jinan, Jinan 250022, PR China

[b] Key Laboratory of Optic-electric Sensing and Analytical Chemistry for Life Science, MOE; Shandong Key Laboratory of Biochemical Analysis; Key Laboratory of Analytical Chemistry for Life Science in Universities of Shandong; College of Chemistry and Molecular Engineering, Qingdao University of Science and Technology, Qingdao 266042, PR China

[c] School of Water Conservancy and Environment, University of Jinan, Jinan 250022, PR China

ARTICLE INFO

Keywords:
Electrochemical immunosensor
Zeolitic imidazolate frameworks
Prostate-specific antigen
Palladium nanoparticles

ABSTRACT

A sandwich-type electrochemical immunosensor for prostate-specific antigen (PSA) detection was constructed. In this sensing platform, palladium nanoparticles (Pd NPs) loaded electroactive amino-zeolitic imidazolate framework-67 (Pd/NH_2-ZIF-67) nanocomposite is utilized as a novel redox mediator. Pd NPs, as the labeling signal molecule, owns good biocompatibility and excellent catalytic performance. Meanwhile, the electroactive ZIF-67 with lamellar structures serves not only as a carrier of Pd NPs but also as a synergistic catalyst of palladium to decompose H_2O_2. Amperometric method is used to determine the current signal generated on the electrode surface, which is conducive to achieve the quantitative determination of PSA. Under optimum conditions, the proposed immunosensor shows a wide detection range from 100 fg mL^{-1} to 50 ng mL^{-1} with a low detection limit of 0.03 pg mL^{-1}, featuring favorable selectivity, repeatability and stability. This proposed immunosensor is expected to be a powerful tool for realizing quantitative detection of PSA and other biomarkers in actural sample analysis.

1. Introduction

Prostate cancer, as a kind of malignant tumor in male prostate tissue, is one of the most common malignant tumor for male around the world (Center et al., 2012). In recent years, the incidence rate of prostate cancer has also shown a trend of significant increase in some developing countries (Chen et al., 2016). Prostate-specific antigen (PSA) is a kind of glycoprotein produced in human prostate tissue, whose content in normal human serum is extremely low. However, the concentration of PSA shows a rising level in the serum of prostate cancer patients (Mahal et al., 2018). Serum PSA detection combined digital rectal examination is the main mode presently recognized for prostate cancer screening (Andriole et al., 2012; Schroder et al., 2009). PSA detection in the asymptomatic male group with potential prostate cancer risk can effectively discover the prostate cancer at an early stage to reduce the related mortality rate and prolong the life-span of patients (Cooperberg et al., 2018). At present, early detection of latent prostate cancer concerned by medical profession can reduce excessive examination and treatment and other frontier problems resulted from PSA screening, and rely more on PSA testing means with high sensitivity and high specificity. Therefore, it will play a crucial role in the early diagnosis, intervention and treatment of prostate cancer to seek PSA testing method with high sensitivity and high specificity.

At present, there are a variety of immune analysis methods for the detection of PSA, mainly including chemiluminescence (Qi et al., 2014), enzyme-linked immunoassay (Lv et al., 2017), fluorescence immunoassay (Kong et al., 2015), electrochemiluminescent immunoassay (Yang et al., 2017), Photoelectrochemistry immunoassay (Pang et al., 2018), SPR Analysis (Ren et al., 2017b) and so on. Notably, electrochemical immunoassay as a product from interdisciplinary development of chemistry, medicine, and biology has attracted extensive attention because of its high sensitivity, strong specificity, rapid response, simple operation, low sample consumption, and low cost. There have been several electrochemical immunosensors designed for the detection of PSA. For example, Yan et al. reported an electrochemical immunosensor based on a screen-printed electrode, which has superiority in facile preparation, low cost, and miniaturization for point-of-care testing or field detection (Lin et al., 2008; Yan et al., 2012). But it

* Corresponding author.

https://doi.org/10.1016/j.bios.2019.02.055
Received 29 November 2018; Received in revised form 17 February 2019; Accepted 18 February 2019
Available online 04 March 2019
0956-5663/

was less than perfect in some ways of instability. Chuah et al. designed a horseradish peroxidase (HRP)-labeled electrochemical immunosensor, it can amplify signals properly, still the enzyme had the disadvantage of easy deactivation (Chuah et al., 2012; Kavosi et al., 2015). Chen et al. proposed a label-free electrochemical immunosensor with concise labeling processes and a higher inspection speed, but the antigen nonspecific adsorption caused false positive events, decreasing the accuracy and sensitivity of the assays (Chen et al., 2019a, 2019b; Oliveira et al., 2018).

The rapid development of nanomaterials have made their roles in the immunosensing field increasingly (Fenzl et al., 2016). The precious metal nano materials, such as gold (Au) (Ma et al., 2017), platinum (Pt) and palladium (Pd) (Wang et al., 2018a) have been widely used in the field of electrochemistry owing to their excellent chemical stability, biocompatibility and catalytic activity. In addition, because of its large specific surface area, and uniform and adjustable pore size (Li et al., 2012), metal organic frameworks (MOFs) materials have been considered to have great application value in adsorption (Liu et al., 2018), storage (He et al., 2017), catalysis (Zhang et al., 2018a) and other areas (Dietzel and Kitagawa, 2016). As a kind of special MOF materials (Eddaoudi et al., 2015), zeolitic imidazolate frameworks (ZIFs) is similar to the Si-O-Si bond angle (145°) of zeolite structure (Jiang and Yaghi, 2015). This kind of special zeolite-like structure can make it have both the high stability of inorganic zeolite and the high porosity of MOFs materials (Houndonougbo et al., 2013).

In this paper, a sandwich-type electrochemical immunosensor based on Pd/NH_2-ZIF-67 nanocomposite is constructed for PSA detection. First of all, gold nanoparticles (Au NPs) are used for modification on the electrode surface by electrodeposition method, and then primary antibodies (Ab_1) was immobilized onto the electrode surface by virtue of the Au-NH_2 bond formed by amino (-NH_2) on Ab_1 and Au NPs (Ren et al., 2017a; Zhang et al., 2018c). Secondly, Pd NPs were loaded on the electroactive NH_2-ZIF-67 as the signal biomarker by virtue of the Pd-NH_2 bond. Pd/NH_2-ZIF-67 nanocomposite is used as the redox probes due to the good biocompatibility, excellent H_2O_2 catalytic performance of Pd NPs (Li et al., 2016) and large specific surface area of ZIF-67. Meanwhile, the electroactive ZIF-67 serves not merely as carriers of Pd NPs but also as synergistic catalyst of palladium to decompose H_2O_2 effectively. In order to enhance the signal output, ZIF-67 is prepared by an improved synthetic step, which makes lamellar stacking structures formed on its surface to increase the specific surface area, and to load more Pd NPs for signal amplification. The secondary antibodies (Ab_2) was connected to the signal biomarker via Pd-NH_2 bond. Finally, the sandwich-type electrochemical immunosensor was created based on the antigen-antibody specific binding reaction on the electrode surface (Ren et al., 2018a). Compared with the published electrochemical immunosensors above, the key advantage of this sandwich-type electrochemical immunosensor is that, the response signal is amplified by synergistic catalysis of ZIF-67 and Pd, and this signal amplification effect can provide with a relatively wide detection range and low detection limit for PSA. Meanwhile, the Pd/NH_2-ZIF-67 nanocomposite of this immunosensor can effectively avoid the antigen nonspecific adsorption and enzyme deactivation, mitigate the environmental impact on the sensor performance, and improve the sensor stability.

2. Experimental

2.1. Material and reagents

Cobaltous nitrate hexahydrate ($Co(NO_3)_2{\cdot}6H_2O$) and 2-methylimidazole (H-MeIM) are obtained from Shanghai Macklin Biochemical Co., Ltd. Methanol (AR) and ethanol (AR) are purchased from Tianjin Fuyu Fine Chemical Co., Ltd. Ammonia, ethylene glycol, Sodium borohydride ($NaBH_4$) and Hydrogen peroxide (30 wt%) are obtained from Sinopharm Chemical Reagent Co., Ltd. Sodium tetrachloropalladate (II) (Na_2PdCl_4), gold chloride ($HAuCl_4$) and sodium citrate are purchased from Bide Pharmatech Ltd. Bovine serum albumin (BSA, 96–99%) is obtained from Aladdin Industrial Corporation. PSA and PSA antibody (Ab) are obtained from Shanghai Linc-Bio Science Co., Ltd (Shanghai, China). Phosphate buffered saline (PBS) is prepared by using Na_2HPO_4 (1/15 mol L^{-1}) and KH_2PO_4 (1/15 mol L^{-1}) solution. $K_3Fe(CN)_6$/$K_4Fe(CN)_6$ (2.5 mmol L^{-1}) and KNO_3 (0.1 mol L^{-1}) solution are used as electrolyte for electrochemical impedance spectroscopy (EIS). Ultrapure water (18.25 MΩ cm, 24 °C) is used for all of the experiments.

2.2. Apparatus

All electrochemical performance measurements are tested on a CHI760D electrochemical workstation (Chenhua Instrument Shanghai Co., Ltd, China). Scanning electron microscope (SEM) images and Energy dispersive spectroscopy (EDS) spectrum are obtained using a field emission SEM (Zeiss, Germany). The surface-areas and porosity analyzer of the samples are obtained by Brumauer–Emmett–Teller (BET, Micromeritics Instrument Corporation, USA). X-Ray Powder Diffraction (XRD) is performed using a D8 advance X-ray diffractometer (Bruker AXS, Germany) from 5° to 60°. The X-ray photoelectron spectroscopy (XPS) measurements are performed on an ESCALABMK II X-ray photoelectron spectrometer using Mg as the excitation source.

2.3. Synthesis of electroactive NH_2-ZIF-67 nanocrystal

The synthesized method of ZIF-67 crystal is reported by Hu et al. (2015), and the synthetic steps are improved for preparation of electroactive ZIF-67 crystal. In details, $Co(NO_3)_2{\cdot}6H_2O$ (4.657 g, 16 mmol) and H-MeIM (3.941 g, 48 mmol) were dissolved into 200 mL methanol solution respectively. And $Co(NO_3)_2$ solution was dropwise added into H-MeIM solution, then it was stirred continuously for 2 min to make the solution mixed evenly. The crystalline precipitation was collected by centrifugation (9000 r min^{-1}, 10 min) and washed by alcohol for several times after it was stable at room temperature for 24 h. The collected centrifuged material was dried in the vacuum drying oven at 60 °C for 12 h, and the product of ZIF-67 was obtained.

To prepare the NH_2-ZIF-67 (Ren et al., 2014), 100 mg of ZIF-67 was added to 40 mL of ethylene glycol under ultrasonication. After further addition of 1 mL of ammonia water, the dark blue solution was transferred to a Teflon lined autoclave for solvothermal reaction at 180 °C for 10 h. After the reaction, the precipitate was collected by centrifugation (9000 r min^{-1}, 10 min), washed repeatedly with distilled water, and dried at 60 °C for 24 h for further usage.

2.4. Preparation of Pd/NH_2-ZIF-67

Pd NPs was synthesized by a published method (Yang et al., 2017). First of all, 0.0736 g of Na_2PdCl_4 (0.25 mM) and 0.0735 g of sodium citrate (0.25 mM) were dissolved in 20 mL of ultrapure water, which was followed by adding 0.6 mL of $NaBH_4$ solution (0.01 M) under continuous stirring. After 30 s, black precipitate was obtained, which means Pd NPs were synthesized successfully. The Pd/NH_2-ZIF-67 was prepared by a typical synthese (Wei et al., 2016). The 100 mg NH_2-ZIF-67 was dissolved in 10 mL suspension solution of Pd NPs. Next, the mixture was ultrasoniced and stirred for another 12 h. The prepared product was washed several times with water and ethanol, and then centrifugalized until the supernatant liquid became colorless. The prepared product was put in the vacuum drying oven at 50 °C for 12 h.

2.5. Preparation of Ab_2-Pd/NH_2-ZIF-67 marker

The process of preparing Ab_2-Pd/NH_2-ZIF-67 is shown in Fig. 1A. Ab_2 was immobilized on Pd/NH_2-ZIF-67 through the cross-linking reaction between -NH_2 on Ab_2 and Pd NPs. Ab_2 dispersion solution (1 mL, 1 μg mL^{-1}) was mixed evenly with PBS of Pd/NH_2-ZIF-67 (1 mL, 2.5 mg mL^{-1}) for shock incubation at 4 °C for 12 h, then Ab_2-Pd/NH_2-

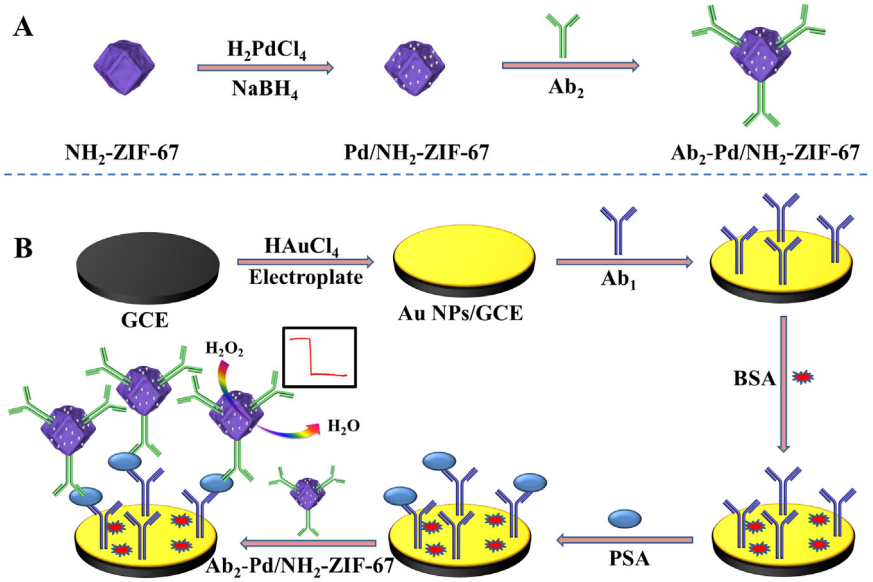

Fig. 1. (A) The illustration of the preparation process of Ab_2-Pd/NH_2-ZIF-67, (B) the preparation processes of the immunosensor.

ZIF-67 was generated, which should be preserved at 4 °C for later use.

2.6. Construction of the immunosensor

The constructing process of electrodes is shown in Fig. 1B. Prior to modified, the glassy carbon electrode (GCE) was polished to mirror face on the polishing cloth by Al_2O_3 powder with diameter of 0.05 μm, then cleaned with ultrapure water. Then the polished GCE was dipped in $HAuCl_4$ aqueous solution (10 mg mL^{-1}) to be scanned at a constant voltage (−0.2 V) for 30 s, so as to make Au NPs have electrolytic deposition on GCE surface. Then, 6 μL Ab_1 dispersed solution was dripped on the electrode surface, and Ab_1 was immobilized on the electrode surface with Au-NH_2 for incubation and natural drying at room temperature. And then Ab_1-Au/GCE was obtained. BSA/PBS (0.1 wt%) solution was dripped on the Ab_1-Au/GCE surface to seal the nonspecific sites, and washed out the unreacted BSA with PBS. Then, 6 μL of PSA at different concentrations was dripped onto BSA/Ab_1-Au/GCE surface for incubation and natural drying at room temperature, and gently washed it to remove the uncombined PSA with PBS, and then got PSA/BSA/Ab_1-Au/GCE. Finally, Ab_2-Pd/NH_2-ZIF-67 (6 μL) was dripped on the electrode surface for incubation 30 min at room temperature. Then the Pd/NH_2-ZIF-67 modified sandwich-type immunosensor was obtained. Eventually, it was kept at 4 °C for later use.

2.7. Electrochemical characterization and measurement

The three-electrode system was used in the electrochemical measurement, in which GCE served as the working electrode, saturated calomel electrode (Hg/$HgCl_2$) was the reference electrode and platinum electrodes served as the counter electrodes. Electrochemical impedance spectroscopy (EIS) was used to characterize the electrochemical characteristics of electrodes in the process of modification. Amperometric measurement (constant voltage −0.4 V vs. Hg/$HgCl_2$) was used for PSA determination (Fig. S1), and PBS (10 mL) was used as the test matrix solution. Under the condition of stirring, after H_2O_2 solution (10 μL, 15 wt%) was quickly added to the matrix solution when the background current was stable, and then recorded the current response value of electrodes to H_2O_2 after it was stable again.

3. Results and discussion

3.1. Characterization of electroactive NH_2-ZIF-67 and Pd/NH_2-ZIF-67

Fig. 2 shows the XRD, SEM and BET characterizations of electroactive NH_2-ZIF-67 and the EDS elemental mapping of Pd/NH_2-ZIF-67. As shown in Fig. 2A, the XRD pattern obtained from experiment is in conformity with the simulated peak position (Qian et al., 2012), and the strongest diffraction peak and stronger appears at about 7.32°, 12.7° and 18° respectively, showing that the electroactive NH_2-ZIF-67 is synthesized successfully.

Fig. 2B shows the SEM image of electroactive ZIF-67. The electroactive ZIF-67 is a polyhedron with hexagonal outline, and the crystal size is about 500 nm. In the synthetic method, we improved the traditional synthetic method of quickly adding H-MeIM to $Co(NO_3)_2$, and Co $(NO_3)_2$, but slowly adding $Co(NO_3)_2$ into H-MeIM, so as to make the generated electroactive ZIF-67 crystal form more lamellar structures on the surface, so as to provide a larger surface area to load more Pd NPs, thus improving the sensitivity of immunosensor. Fig. 2C is the BET characterization diagram of electroactive ZIF-67, in which the electroactive ZIF-67 shows a rapid initial adsorption rate when relative pressure $P/P_0 < 0.1$, and basically reaches adsorption equilibrium when $P/P_0 = 0.1$, which belongs to type I adsorption isotherm, and has the pore structure characteristic given priority to micropores, and the pore size distribution diagram shows that its average pore diameter is 5.2 nm. The specific surface area of electroactive ZIF-67 is 1254.9 $m^2 \cdot g^{-1}$, indicating adsorption property of the prepared electroactive ZIF-67.

XPS is used to characterize the as-synthesized NH_2-ZIF-67. Fig. S2 in the Supporting information (SI) is the XPS survey spectrum for electroactive NH_2-ZIF-67, which illustrates the NH_2-ZIF-67 crystal consisting of Co, O, N and C elements. The Co 2p spectra (Fig. S3) show a doublet containing a low energy band (Co $2p_{3/2}$) and a high-energy band (Co $2p_{1/2}$) at 781.1 and 796.9 eV, respectively. The energy difference between Co $2p_{3/2}$ and Co $2p_{1/2}$ splitting is approximately 15 eV, which indicates the presence of both Co^{2+}/Co^{3+} species in electroactive NH_2-ZIF-67 (Ren et al., 2018b). While the peaks of N 1s spectra (Fig. S4) at 398.9 eV and 400.4 eV correspond to $–NH_2$ and organic matrix (Moulder et al., 1992), respectively. The XPS peak area intensity ratio for $–NH_2$/organic matrix is approximately 3.1, indicating that $–NH_2$ exists in the surface of electroactive NH_2-ZIF-67.

The SEM image and EDS elemental mapping images of Pd/NH_2-ZIF-67 are provided in Fig. 2D, E and F, respectively. It was observed that

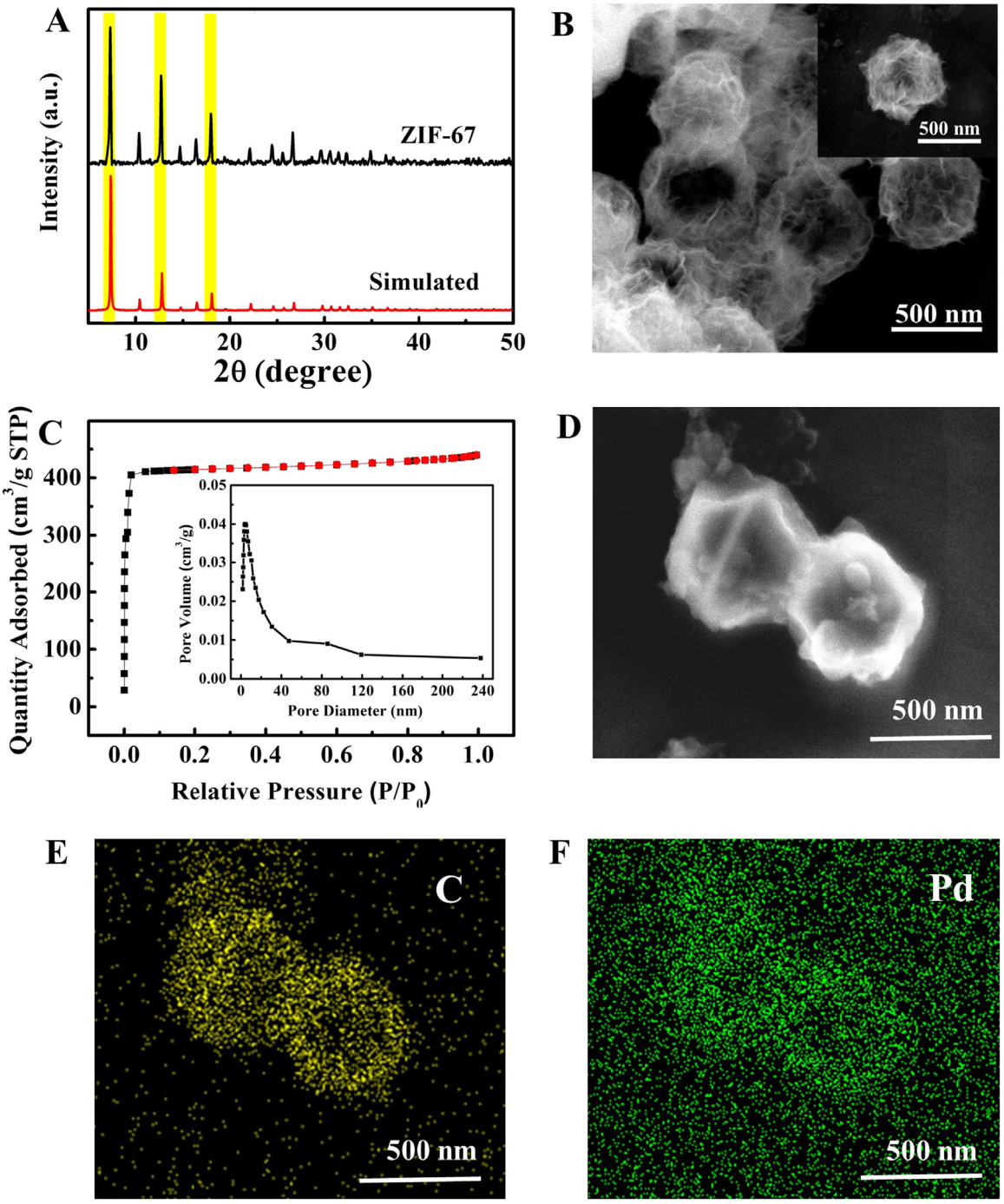

Fig. 2. (A) The XRD patterns of electroactive ZIF-67 (Black line) and the simulated peak of ZIF-67 (red line) patterns. (B) SEM image of electroactive ZIF-67. (C) N_2 adsorption and desorption isotherms of electroactive ZIF-67 and corresponding pore size distribution curve. (D) SEM image of Pd/NH_2-ZIF-67. (E) and (F) EDS elemental mapping were implemented to characterize dispersion of Pd in the NH_2-ZIF-67 crystal. (For interpretation of the references to color in this figure legend, the reader is referred to the web version of this article).

particles uniformly distributed on the lamellar structures, showing that Pd NPs has been loaded on electroactive NH_2-ZIF-67. EDS is employed to further analyze the chemical composition of the Pd/NH_2-ZIF-67 (Fig. S5). While XRD pattern of Pd/NH_2-ZIF-67 also exhibits a diffraction peak of Pd NPs at about 40° (Fig. S6). The above characterizations show that Pd/NH_2-ZIF-67 has been successfully prepared.

3.2. Electrochemical characterization of immunosensor

The electrochemical impedance spectroscopy (EIS) complex plane of electrode at different modification phases in $K_3Fe(CN)_6$/KCl solution is shown in Fig. 3 The changes in size of capacitive reactance arc can reflect the impedance change on electrode surface (Ren et al., 2017c; Zhang et al., 2018b). Bare GCE shows a small capacitive reactance arc (curve a). Due to the strong electron transfer ability of Au, the Au/GCE impedance spectrum is almost a straight line (curve b) in the whole frequency range. When Ab_1, BSA, PSA, and Ab_2-Pd/NH_2-ZIF-67 was gradually used to modify on Au/GCE surface, the capacitive reactance increase gradually (curve c-f) along with the modification of electrodes layer by layer owing to the inhibition effect of each modification layer

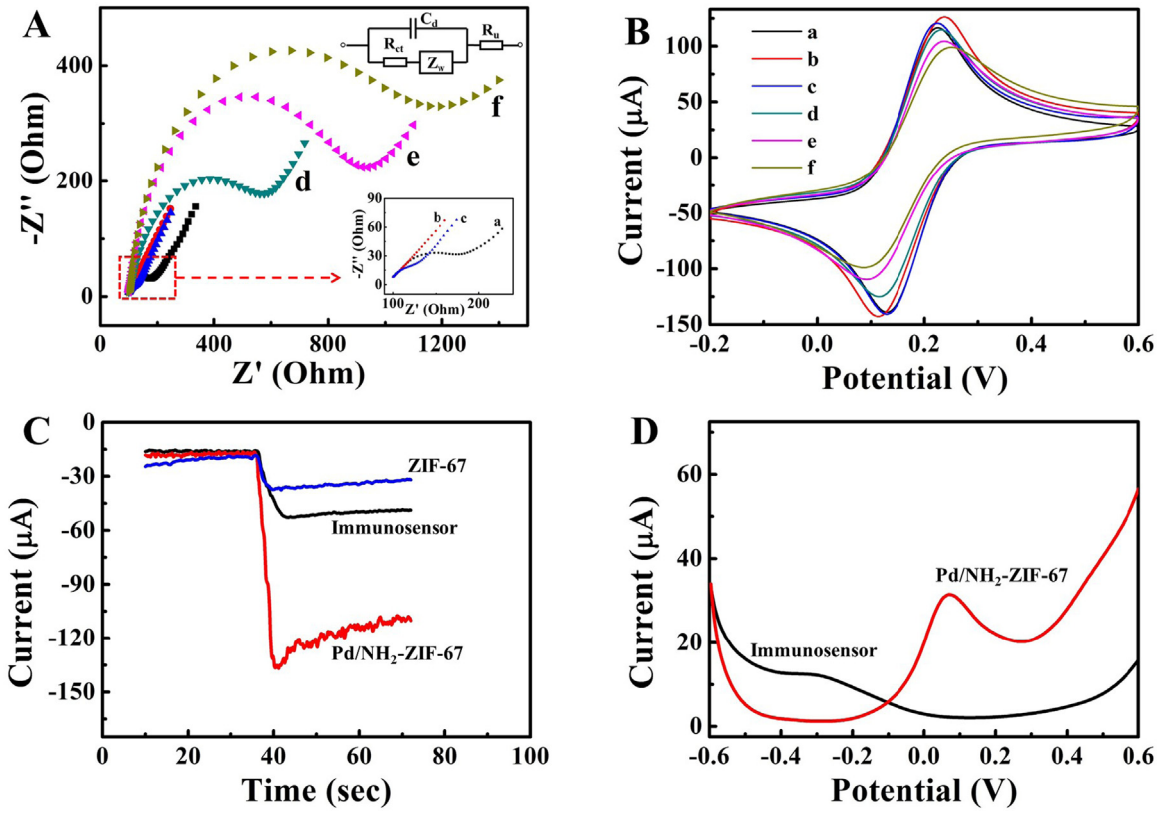

Fig. 3. (A) EIS and (B) CV of all modifiers used for the immunosensor fabrication in 1 mmol L^{-1} $[Fe(CN)_6]^{3-/4-}$ and 0.1 mol L^{-1} KCl. (a) GCE, (b) Au/GCE, (c) Ab_1-Au/GCE, (d) BSA/Ab_1-Au/GCE, (e) PSA/BSA/Ab_1-Au/GCE and (f) Ab_2-Pd/NH_2-ZIF-67/PSA/BSA/Ab_1-Au/GCE. (C) Amperometric curve of the immunosensor for the detection of different modifier step of PSA (blue curve) NH_2-ZIF-67/GCE; (red curve) Pd/NH_2-ZIF-67/GCE; (black curve) electrode was modified completely as an immunosensor. (D) DPV response of the Pd/NH_2-ZIF-67/GCE (red curve) and the immunosensor (black curve). (For interpretation of the references to color in this figure legend, the reader is referred to the web version of this article).

on the diffusion of probe molecules $[Fe(CN)_6]^{3-/4-}$ on the surface of electrodes, indicating the electrochemical immunosensor has been successfully built.

Meanwhile, the cyclic voltammetry (CV) was used to further investigate the assembly course of the immunosensor. CVs were tested in 5 mmol L^{-1} $[Fe(CN)_6]^{3-/4-}$ solution at 100 mV/s (Fig. 3B). Bare GCE (curve a) shows a smaller current than the Au NPs/GCE (curve b), for the better conductive ability of Au NPs. Because the immunosensor can severely increase the steric hindrance, the current dramatically decreases after PSA Ab_1 was assembled onto the electrode surface (curve c), demonstrating the successful modification of Ab_1. Then the current decreases further (curve d) after the electrode was incubated with BSA. This is because BSA makes a blockage of electronic transportation. After the electrode was modified stepwise with PSA and Ab_2-Pd/NH_2-ZIF-67, the peak current was gradually decreased (curve e and f), which is due to the specific binding between anti-PSA antibody and PSA that retards the electron-transfer.

On the other hand, the electroactive NH_2-ZIF-67 had not only the amperometric signal but also the differential pulse voltammetry (DPV) signal in the catalysis field of H_2O_2. Accordingly, selecting an appropriate measurement pattern is essential. As shown in Fig. 3C, the amperometric responses of NH_2-ZIF-67 increases after loading Pd NPs. When finished the modification of the immunosensor, the amperometric signal decreases compared with the Pd/NH_2-ZIF-67, due to the inevitable strong charge transfer impedance of antigen-antibody and BSA on the electrode surface. However, there still a certain intensity of amperometric signal can be detected. As shown in Fig. 3D, when the Pd/NH_2-ZIF-67 was modified on the electrode surface, a DPV peak was exhibited. However, the DPV signal almost disappeared after the immunosensor is fabricated well. Thus, it is suitable to take amperometric method as a measurement pattern.

3.3. Optimization of conditions for immunosensor

The performance of immunosensor is influenced by many factors, of which pH has a great influence on the protein structure and activity (Wang et al., 2018b). Amperometric measurement is used in this experiment to test the current signal response situation of immunosensor in PBS at different pH (5.3–8.4) values, and the electrodes used for pH selection test are the immunosensors built based on the modification by PSA at 5 ng mL^{-1} and Ab_2-Pd/NH_2-ZIF-67 at 1 mg mL^{-1} on BSA/Ab_1-Au/GCE. As shown in Fig. 4A, when pH = 5.3–7.4, the current response of the immunosensor enhanced with the increase of pH; when pH = 7.4–8.4, the response signal was weakened along with the increase of pH; the response signal is strongest at pH = 7.4. Therefore, pH = 7.4 in this experiment is the optimal condition of the immunosensors.

The modification of electrodes by Pd/NH_2-ZIF-67 can directly affect the sensitivity of immunosensor, so it is necessary to optimize the modification concentration of Pd/NH_2-ZIF-67. In the process of building the immunosensor, PSA at 5 ng mL^{-1} and Pd/NH_2-ZIF-67 at different concentrations (0.25–1.75 mg mL^{-1}) is used for modification on immuno-electrodes BSA/Ab_1-Au NPs/GCE, and the test is done at the optimal PBS (pH = 7.4). As shown in Fig. 4B, the response signal of Ab_2-Pd/NH_2-ZIF-67 at the concentration of 0.25–1.25 mg mL^{-1} is enhanced with the increase of its concentration, but it shows an unstable fluctuating change after 1.25 mg mL^{-1}. Therefore, the concentration of 1.25 mg mL^{-1} is selected as the optimal incubation concentration of Ab_2-Pd/NH_2-ZIF-67. Additionally, electrodeposition time is another critical criterion to evaluate the economic and time cost of

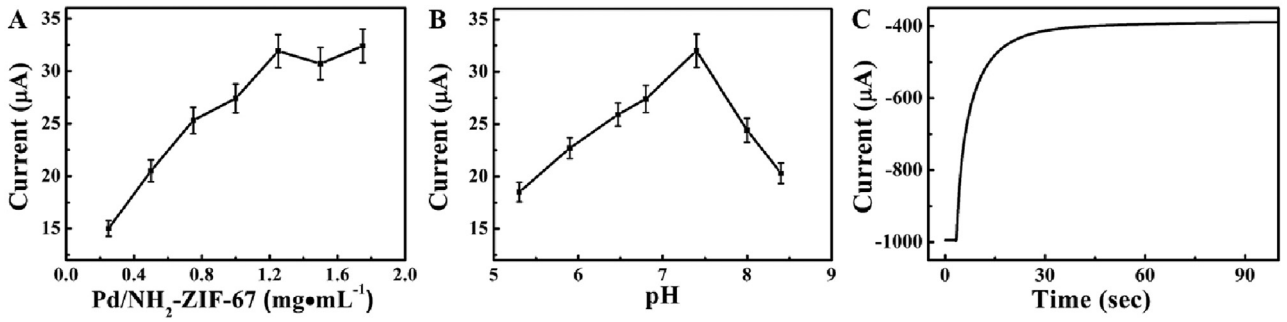

Fig. 4. (A) The effect of Pd/NH_2-ZIF-67 concentrations on the immunosensor for detection 5 ng mL^{-1} PSA, Error bars = SD (n = 5). (B) The effect of pH on the response of current signal intensity from sensors, Error bars = RSD (n = 5). (C) The effect of electrodeposition time (voltage = −0.2 V).

immunosensor. As shown in Fig. 4C, when the current responses of the electrodeposition process increase to a higher level at 30 s, the current responses have remained approximately constant after 30 s. Therefore, electrodeposition 30 s is selected as the optimal electrodeposition time of electrode to obtain the best configuration of time and resource.

3.4. Research on immunosensor performance

Under the optimum conditions, the electrochemical immunosensor is tested with amperometric measurements (constant voltage −0.4 V), and the i~t curve is shown in Fig. 5A, demonstrating that the response current signal (curve a~j) enhances with the increase of concentration of PSA within the scope of 0 ng mL^{-1}~50 ng mL^{-1}. As shown in Fig. 5B, the logarithm between the timing current response value of immunosensor and PSA concentration maintains a good linear positive correlation. Its linear regression equation within the concentration scope: $\Delta I = 28.326 + 4.78\lg c$, R = 0.991, and the detection limit is 0.03 pg mL^{-1}. The electrodeposition Au NPs at the matrix exhibits good biological compatibility and strong electron transfer capability. The electroactive NH_2-ZIF-67 has a higher specific surface area and excellent adsorption to load more Pd NPs. These characteristics are conductive to improve the sensitivity of immunosensor, thus leading a lower detection limit. Compared with previous reports (Table S2), the proposed biosensor shows a more excellent detection limit (0.03 pg mL^{-1}) and liner range from 100 fg mL^{-1} to 50 ng mL^{-1}.

3.5. Selectivity, repeatability and stability

The important parameters to evaluate the performance of electrochemical immunosensor are selectivity, repeatability and stability. BSA, Human immunoglobulin G (HIgG), Ascorbic Acid (AA), Hepatitis B surface antigen (HBsAg) and Glucose contained in human serum are respectively used as the interfering substances to test the selectivity of immunosensors. The test is divided into 6 groups, and each group is tested for 5 times. The first group is PSA at 1 ng mL^{-1}, and the other five groups are PSA at 1 ng mL^{-1} added with the interfering substances above at 100 ng mL^{-1} respectively. As shown in Fig. 6A, the relative standard deviation (RSD) among the 6 groups is 3.94% in the presence of interfering substances, which shows that the built immunosensor has good selectivity.

Under the optimum conditions, five fabricated immunosensors are used to detect the PSA at 0.1 ng mL^{-1}. In Fig. 6B, the RSD of its response current signal value is 2.60%. After the immunosensors are preserved in the refrigerator at 4 °C for 4 weeks, as shown in Fig. 6C, the response current signal value is greater than 94% of that of original signal, demonstrating that this immunosensor has good stability and repeatability.

3.6. Application of the developed immunosensor

Specimens from normal human serum, added PSA standard solution after it was diluted twice, prepared the standard samples at different concentrations, and conducted standard addition recovery test on the immunesensor prepared in this paper at the concentrations of 0.1, 0.2, 0.5, 1.0, 5.0 and 10.0 ng mL^{-1}. PSA content determination results are shown in Table S3. The RSD is 1.1–4.9%, and the recovery rate is 94–105%. The results show that this immunosensor is provided with a good detection performance on spiked samples, thus leading to a higher reference value for clinical detection.

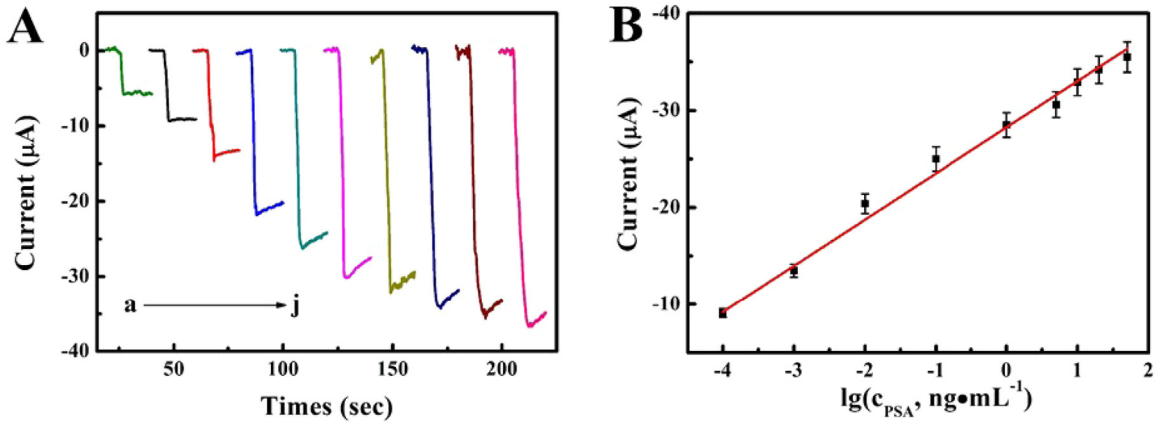

Fig. 5. (A) Amperometric response of the biosensor to different concentrations of PSA, from a to j: 0.0, 0.0001, 0.001, 0.01, 0.1, 1, 5, 10, 20, and 50 ng mL^{-1}. (B) Calibration curve of the biosensor for different concentrations of PSA (the response current intensity is 5.8 μA in the 0 ng mL^{-1} PSA solution).

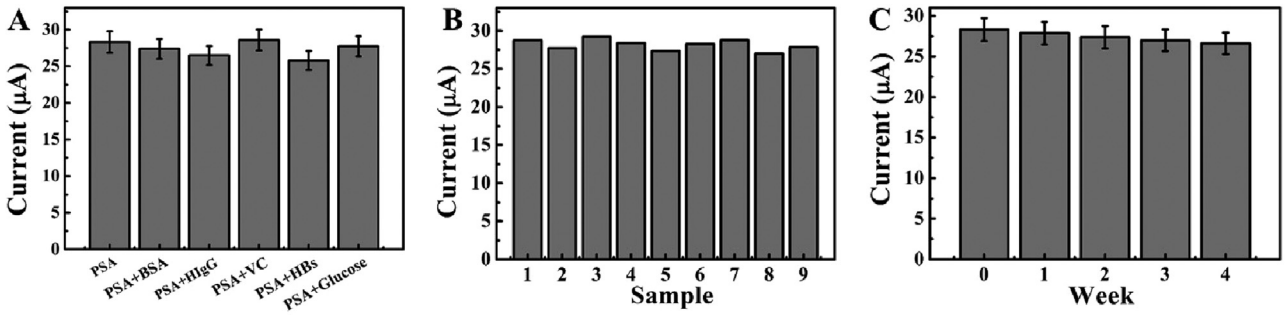

Fig. 6. (A) The concentrations of the interference species are PSA (1 ng mL^{-1}), 100 ng mL^{-1} of (BSA, HIgG, AA, HBs, Glucose), error bar = RSD (n = 5). (B) The response of the immunosensor to detection of 1 ng mL^{-1} PSA. (C) The stability of the AFP immunosensor, error bar = RSD (n = 5).

4. Conclusion

In summary, a highly sensitive electrochemical immunosensor using Pd/NH_2-ZIF-67 as the signal-amplification inducer is constructed for the quantitative determination of PSA in spiked human serum. ZIF-67 synthesized by the improved method can expose more active sites due to its larger specific surface area, which is conducive for the bond of Pd NPs on its surface. Pd/NH_2-ZIF-67 composite as the signal indicator plays an important role in realizing favorable signal amplification due to the excellent synergetic catalytic effect between Pd and NH_2-ZIF-67. Moreover, a linear range from 100 fg·mL^{-1} to 50 ng mL^{-1} with a low detection limit of 0.03 pg mL^{-1} is achieved for detecting PSA. In addition, owing to the advantages of satisfying reproducibility, stability and specificity this approach probably provided a promising opportunity for clinical diagnosis. However, there're still some points to be improved, such as miniaturization (Ainla et al., 2018) and portability (Li et al., 2017) of the device, enhancing the integration level of the technic (Chen et al., 2019a, 2019b), which points out the direction for further research.

CRediT authorship contribution statement

Li Dai: Conceptualization, Data curation, Investigation, Project administration, Supervision, Validation, Writing - original draft. **Yueyuan Li:** Conceptualization, Project administration, Supervision, Validation. **Yaoguang Wang:** Supervision, Validation, Writing - review & editing. **Xiliang Luo:** Supervision, Validation, Writing - review & editing. **Dong Wei:** Supervision, Validation, Writing - review & editing. **Rui Feng:** Supervision, Validation, Writing - review & editing. **Tao Yan:** Supervision, Validation, Writing - review & editing. **Xiang Ren:** Supervision, Validation, Writing - review & editing. **Bin Du:** Supervision, Validation, Writing - review & editing. **Qin Wei:** Conceptualization, Project administration, Supervision, Validation.

Acknowledgements

This study was supported by the National Natural Science Foundation of China (Nos. 201505051 and 21575050), National Key Scientific Instrument and Equipment Development Project of China (No. 21627809).

Declaration of interests

None.

Appendix A. Supplementary material

Supplementary data associated with this article can be found in the online version at doi:10.1016/j.bios.2019.02.055.

References

Ainla, A., Mousavi, M.P.S., Tsaloglou, M.N., Redston, J., Bell, J.G., Fernandez-Abedul, M.T., Whitesides, G.M., 2018. Anal. Chem. 90 (10), 6240–6246.
Andriole, G.L., Crawford, E.D., Grubb 3rd, R.L., Buys, S.S., Chia, D., Church, T.R., Fouad, M.N., Isaacs, C., Kvale, P.A., Reding, D.J., Weissfeld, J.L., Yokochi, L.A., O'Brien, B., Ragard, L.R., Clapp, J.D., Rathmell, J.M., Riley, T.L., Hsing, A.W., Izmirlian, G., Pinsky, P.F., Kramer, B.S., Miller, A.B., Gohagan, J.K., Prorok, P.C., Team, P.P., 2012. J. Natl. Cancer Inst. 104 (2), 125–132.
Center, M.M., Jemal, A., Lortet-Tieulent, J., Ward, E., Ferlay, J., Brawley, O., Bray, F., 2012. Eur. Urol. 61 (6), 1079–1092.
Chen, W., Zheng, R., Baade, P.D., Zhang, S., Zeng, H., Bray, F., Jemal, A., Yu, X.Q., He, J., 2016. CA Cancer J. Clin. 66 (2), 115–132.
Chen, C.A., Yeh, W.S., Tsai, T.T., Li, Y.D., Chen, C.F., 2019a. Lab Chip 19 (4), 598–607.
Chen, Y., Yuan, P.X., Wang, A.J., Luo, X., Xue, Y., Zhang, L., Feng, J.J., 2019b. Biosens. Bioelectron. 126, 187–192.
Chuah, K., Lai, L.M., Goon, I.Y., Parker, S.G., Amal, R., Justin Gooding, J., 2012. Chem. Commun. (Camb.) 48 (29), 3503–3505.
Cooperberg, M.R., Brooks, J.D., Faino, A.V., Newcomb, L.F., Kearns, J.T., Carroll, P.R., Dash, A., Etzioni, R., Fabrizio, M.D., Gleave, M.E., Morgan, T.M., Nelson, P.S., Thompson, I.M., Wagner, A.A., Lin, D.W., Zheng, Y., 2018. Eur. Urol. 2, 211–217.
Dietzel, P.D.C., Kitagawa, H., 2016. Eur. J. Inorg. Chem. 2016 (27), 4273–4274.
Eddaoudi, M., Sava, D.F., Eubank, J.F., Adil, K., Guillerm, V., 2015. Chem. Soc. Rev. 44 (1), 228–249.
Fenzl, C., Hirsch, T., Baeumner, A.J., 2016. TrAC Trends Anal. Chem. 79, 306–316.
He, Q., Liu, J., Li, Z., Li, Q., Xu, L., Zhang, B., Meng, J., Wu, Y., Mai, L., 2017. Small 13 (37), 1701504.
Houndonougbo, Y., Signer, C., He, N., Morris, W., Furukawa, H., Ray, K.G., Olmsted, D.L., Asta, M., Laird, B.B., Yaghi, O.M., 2013. J. Phys. Chem. C 117 (20), 10326–10335.
Hu, H., Guan, B., Xia, B., Lou, X.W., 2015. J. Am. Chem. Soc. 137 (16), 5590–5595.
Jiang, J., Yaghi, O.M., 2015. Chem. Rev. 115 (14), 6966–6997.
Kavosi, B., Salimi, A., Hallaj, R., Moradi, F., 2015. Biosens. Bioelectron. 74, 915–923.
Kong, R.M., Ding, L., Wang, Z., You, J., Qu, F., 2015. Anal. Bioanal. Chem. 407 (2), 369–377.
Li, H., Zhao, B., Ding, R., Jia, Y., Hou, H., Fan, Y., 2012. Cryst. Growth Des. 12 (8), 4170–4179.
Li, Y., Tian, L., Liu, L., Liu, L., Li, J., Wei, Q., Cao, W., 2016. New. J. Chem. 40 (1), 558–563.
Li, Z., Li, F., Xing, Y., Liu, Z., You, M., Li, Y., Wen, T., Qu, Z., Ling Li, X., Xu, F., 2017. Biosens. Bioelectron. 98, 478–485.
Lin, Y.Y., Wang, J., Liu, G., Wu, H., Wai, C.M., Lin, Y., 2008. Biosens. Bioelectron. 23 (11), 1659–1665.
Liu, J., Zheng, J., Barpaga, D., Sabale, S., Arey, B., Derewinski, M.A., McGrail, B.P., Motkuri, R.K., 2018. Eur. J. Inorg. Chem. 2018 (7), 885–889.
Lv, S., Li, Y., Zhang, K., Lin, Z., Tang, D., 2017. ACS Appl. Mater. Interfaces 9 (44), 38336–38343.
Ma, H., Zhao, Y., Liu, Y., Zhang, Y., Wu, D., Li, H., Wei, Q., 2017. Anal. Chem. 89 (24), 13049–13053.
Mahal, B.A., Yang, D.D., Wang, N.Q., Alshalalfa, M., Davicioni, E., Choeurng, V., Schaeffer, E.M., Ross, A.E., Spratt, D.E., Den, R.B., Martin, N.E., Mouw, K.W., Orio 3rd, P.F., Choueiri, T.K., Taplin, M.E., Trinh, Q.D., Feng, F.Y., Nguyen, P.L., 2018. Eur. Urol. 36, 7735–7744.
Moulder, J.F., Stickle, W.F., Sobol, P.E., Bomben, K.D., 1992. Perkin-Elmer Corporation: Eden Prairie.
Oliveira, N., Costa-Rama, E., Viswanathan, S., Delerue-Matos, C., Pereira, L., Morais, S., 2018. Electroanalysis 30 (11), 2604–2611.
Pang, X., Cui, C., Su, M., Wang, Y., Wei, Q., Tan, W., 2018. Nano. Energy 46, 101–109.
Qi, H., Li, M., Dong, M., Ruan, S., Gao, Q., Zhang, C., 2014. Anal. Chem. 86 (3), 1372–1379.
Qian, J., Sun, F., Qin, L., 2012. Mater. Lett. 82, 220–223.
Ren, X., Lu, P., Feng, R., Zhang, T., Zhang, Y., Wu, D., Wei, Q., 2018a. Talanta 188, 593–599.
Ren, X., Ma, H., Zhang, T., Zhang, Y., Yan, T., Du, B., Wei, Q., 2017a. ACS Appl. Mater. Interfaces 9 (43), 37637–37644.
Ren, X., Wu, D., Ge, R., Sun, X., Ma, H., Yan, T., Zhang, Y., Du, B., Wei, Q., Chen, L., 2018b. Nano Res. 11 (4), 2024–2033.

Ren, X., Yan, J., Wu, D., Wei, Q., Wan, Y., 2017b. ACS Sens. 2 (9), 1267–1271.
Ren, X., Yan, T., Zhang, Y., Wu, D., Ma, H., Li, H., Du, B., Wei, Q., 2014. Biosens. Bioelectron. 58, 345–350.
Ren, X., Zhang, T., Wu, D., Yan, T., Pang, X., Du, B., Lou, W., Wei, Q., 2017c. Biosens. Bioelectron. 94, 694–700.
Schroder, F.H., Hugosson, J., Roobol, M.J., Tammela, T.L., Ciatto, S., Nelen, V., Kwiatkowski, M., Lujan, M., Lilja, H., Zappa, M., Denis, L.J., Recker, F., Berenguer, A., Maattanen, L., Bangma, C.H., Aus, G., Villers, A., Rebillard, X., van der Kwast, T., Blijenberg, B.G., Moss, S.M., de Koning, H.J., Auvinen, A., Investigators, E., 2009. N. Engl. J. Med. 360 (13), 1320–1328.
Wang, R., Liu, W.D., Wang, A.J., Xue, Y., Wu, L., Feng, J.J., 2018a. Biosens. Bioelectron. 99, 458–463.
Wang, Y., Wang, Y., Wu, D., Ma, H., Zhang, Y., Fan, D., Pang, X., Du, B., Wei, Q., 2018b. Sens. Actuators B: Chem. 255, 125–132.
Wei, Y., Li, Y., Li, N., Zhang, Y., Yan, T., Ma, H., Wei, Q., 2016. Biosens. Bioelectron. 79, 482–487.
Yan, M., Zang, D., Ge, S., Ge, L., Yu, J., 2012. Biosens. Bioelectron. 38 (1), 355–361.
Yang, L., Li, Y., Zhang, Y., Fan, D., Pang, X., Wei, Q., Du, B., 2017. ACS Appl. Mater. Interfaces 9 (40), 35260–35267.
Zhang, B., Gao, W., Piao, J., Xiao, Y., Wang, B., Peng, W., Gong, X., Wang, Z., Yang, H., Chang, J., 2018a. ACS Appl. Mater. Interfaces 10, 14549–14588.
Zhang, T., Ma, N., Ali, A., Wei, Q., Wu, D., Ren, X., 2018a. Biosens. Bioelectron. 119, 176–181.
Zhang, T., Xing, B., Han, Q., Lei, Y., Wu, D., Ren, X., Wei, Q., 2018b. Anal. Chim. Acta 1032, 114–121.